Journal of Mechanical Engineering and Automation 2015, 5(1): 33-42
DOI: 10.5923/j.jmea.20150501.05

Comparative Study of Evolution of Residual Stress State by Local Mechanical Tensioning and Laser Processing of Ferritic and Austenitic Structural Steel Welds

Jibrin Sule[1,*], Supriyo Ganguly[1], Harry Coules[2], Thilo Pirling[3]

[1]Welding Engineering and Laser Processing Centre, Cranfield University, Bedford, UK
[2]Solid Mechanics Research Group, University of Bristol, Bristol, UK
[3]Institut Max von Laue-Paul Langevin, 6 rue Jules Horowitz, Grenoble, France

Abstract Complex thermal stresses generated in welded structures are undesirable but inevitable in fusion welding. The presence of residual stresses can be detrimental to the integrity of a welded joint. In this research, redistribution of residual stress magnitude and profile was studied and compared in two multi-pass welded structural alloys (API X100 and 304L stainless steel) after cold rolling and laser processing. The residual stress field was studied by neutron diffraction using the SALSA strain scanner at their reactor neutron source at ILL, Grenoble. In addition to a complex distribution of residual stress state, multi-pass welds also forms dendritic grain structure, which are repeatedly heated, resulting in segregation of alloying elements. Dendritic grain structure is weaker and segregation of alloying elements may result in formation of corrosion microcells as well as reduction in overall corrosion prevention due to depletion of alloying elements in certain areas. The modification of as-welded residual stress state was done by cold rolling which was followed by laser processing to create a recrystallized microstructure to minimise segregation. The main objective of this study is to understand the suitability of this novel manufacturing technique to create a stress free weldment with recrystallised grain structure. Hardness evolution in the welded structures was scanned following welding, post weld cold rolling and cold rolling followed by laser processing. Hardness distribution in both the structural alloys showed a significant evidence of plastic deformation near the cap pass of the weld metal. Residual stress redistribution was observed up to 4 mm from the capping pass for ferritic steel, while in austenitic steel weld, post weld cold rolling was effective in modifying the residual stress redistribution throughout the entire thickness. Laser processing in both cases reinstated the as-welded residual stress distribution and resulted in softening of the strained area.

Keywords Ferritic and austenitic structural steel, Residual stress, Multi-pass welds, Neutron diffraction, Rolling, Laser processing

1. Introduction

Multi-pass fusion welding by a filler welding electrode is normally carried out to join thick steel sections used in most engineering applications. Welded joints in any installation, is an area of critical importance, since they are likely to contain a higher density of defects than the parent metal and their physical properties can differ significantly from the parent metal. The arc fusion welding relies on intense local heating at a joint where a certain amount of the base metal is melted and fused with additional metal from the filler wire. Intense local heating causes severe thermal gradients in a welded component and the uneven cooling that follows generates residual stresses. The locked-in residual stress is a major concern in structural alloys [1-2]. In multi-pass welds, multiple thermal cycles resulted in a variably distribution of residual stress field across the weld and through the thickness.

While some residual stresses may be beneficial, most are detrimental to the integrity and the service behaviour of the welded part [3]. For example, tensile residual stresses near the weld area have adverse effects in the material. It was reported that tensile welding residual stresses can contribute to fatigue crack development in a structure even under compressive cyclic loading [4-5]. Residual stresses can also affect fracture processes [6-7] and has been reported to accelerate the onset of creep damage [8-10]. This explained why significant resources are devoted to the inclusion of residual stresses in engineering integrity assessments [11], [12-13].

* Corresponding author:
jibrinsule2005@yahoo.com (Jibrin Sule)
Published online at http://journal.sapub.org/jmea

The formation of residual stresses in welded components is compounded by several factors. The contributing factors are (1) structural parameters which include the geometry, size and the joint design; (2) material parameters which reflect the response of a material to the transient thermal cycle; and (3) fabrication parameters include the welding process which determines the heat input, cooling conditions and the restraint applied. Therefore, the thermal response and residual stress generation in these two different structural alloys would be different owing to their difference in physical properties and welding conditions.

Previous investigators have developed several methods to reduce the residual stresses attributed to welding of both ferritic and austenitic steel. These methods include; heat treatment, hammering, preheating, vibration stress relieving, weld sequencing, modification of the structural configurations and the implementation of thermal tensioning techniques [14-18]. The water-shower cooling during welding was also reported to reduce tensile residual stress in austenitic stainless steel welding [19].

In this research, two stages were proposed. In the first step application of high pressure cold rolling on the multi-pass weld. This is done by applying a large compressive force in the direction normal to the welded object's surface cause plastic expansion in the in-plane directions [20]. Although, application of post weld cold rolling to reduce weld residual stress and distortion for a thin plate has been in practice for many years [21-23]. Recent works by Coules et'al [24] and Altenkirch et'al [20] have shown that the post weld cold rolling methods was effective in reducing residual stresses in single pass welds. However, application of this technique on multi-pass welds is not yet reported.

In the second step, laser processing was carried out following the rolling. The purpose of laser processing is to induce recrystallization after cold rolling the weld metal. Weld metal solidifies as dendrites which causes segregation which is specifically prominent in case of high alloyed steel such as austenitic stainless steel. Cold rolling of the weld metal resulted in local plastic deformation which introduces strain energy to relax the tensile residual stress field. Application of laser was intended to induce recrystallization; however, excessive application would result in reinstating the residual stress state which was eliminated during cold rolling.

To the best knowledge of the author, there are no reported works in the literature relating to the application of post weld cold rolling followed by laser processing of weld metal in a multi-pass weld.

The aim of this research is to apply this novel processing to improve structural integrity of multi-pass welds by redistributing locked-in residual stress and creating a recrystallised grain structure minimising segregation generated during solidification of weld metal.

2. Experimental Procedures

2.1. Materials

2.1.1. API X100 Steel Plates

This material was machined to the dimension of 300 × 150 × 20 mm^3 and a narrow groove edge preparation of 5° angle with backing bar was made as shown in Figure 1. The filler wire used was Union MoNi (1.0 mm diameter), while the shielding gas was 92% Ar and 8% O_2 at flow rate of 30 $lit.min^{-1}$. Chemical compositions of the API X100 steel plates and the filler wire are shown in Table 1 and Table 2 respectively.

2.1.2. 304L Stainless Steel Plate

The second material was also machined to the dimension of 300 x 150 x 12 mm^3. The welding preparation is as shown in Figure 1. The filler wire used was Lincoln MIG 308L Si of 1.0 mm nominal diameter. Table 3 shows the chemical compositions of the 304L stainless steel plate. Table 4 shows the chemical compositions of the filler wire. The shielding gas used was 98% Ar and 2% O2 at flow rate of 30 $lit.min^{-1}$.

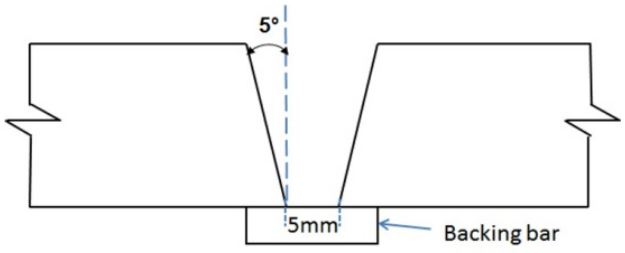

Figure 1. Welding setup preparation with backing bar

Table 1. Composition (wt. %) of the API X100 steel plates

C	Si	Mn	P	Mo	Ni	Al	B	Cu	Nb	Ti	V	Cr	S
0.06	0.25	1.79	0.016	0.16	0.13	0.03	<0.0005	0.27	0.03	0.01	0.04	0.03	<0.003

Table 2. Composition (wt. %) of the filler wire used for API X100 steel

C	Si	Mn	P	Mo	Ni	Cu	Cr	S	Others
0.12	0.4 -0.8	1.3 - 1.9	0.015	0.25 - 0.65	0.8 -1.3	0.3	0.15	0.018	0.25

2.2. Experimental Method

This experiment was carried out in three stages. Firstly, welding using Tandem GMAW DC with electrode positive (DCEP) polarity; post weld cold rolling was done with rolling load up to 150 kN using a local rolling machine, and finally the post weld cold rolling was followed by laser processing using 8 kW fibre laser machine as shown in the flow chart. Microstructural observations, hardness scanning and residual stress measurement were carried out after each stage. The experimental details are shown in figure 2.

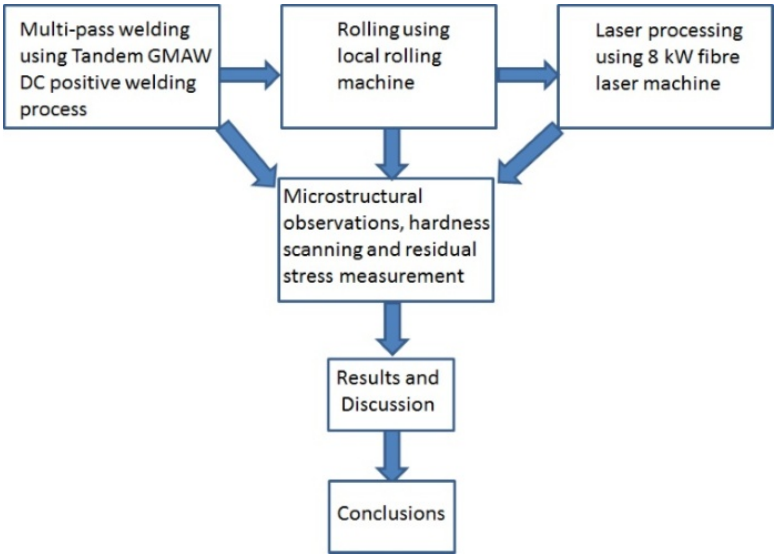

Figure 2. Experimental methodology

Table 3. Composition (wt. %) of the 304L stainless steel plate

C	Si	Mn	Cr	P	Mo	Ni	Al	S	Cu	Nb	Ti
0.021	0.36	1.48	18.2	0.022	0.15	8.10	< 0.01	< 0.005	0.19	0.01	< 0.01

Table 4. Composition (wt. %) of the filler wire used for 304L stainless steel plate

C	Si	Mn	Cr	P	Mo	Ni
0.01	0.75	1.6	20	0.015	0.20	10

2.2.1. Welding

Tandem GMAW DC positive welding process was used for both the alloys. Figure 3 shows the welding torch used. The contact tips were fed by two independent power sources and two independent wire feeding units. A number of researches on this welding process has been reported and can be found in [25-26]. The welding parameters are shown in Table 5 and Table 6 for API X100 steel plates and 304L stainless steel plates respectively.

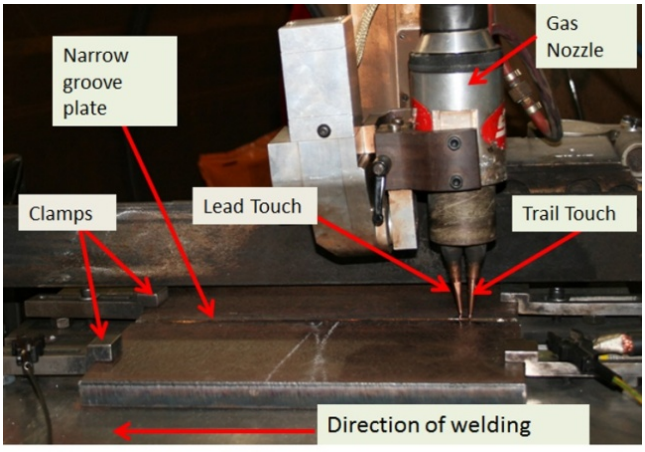

Figure 3. Typical tandem GMAW torch

Table 5. Welding parameters on narrow groove welds of API X100 steel plate

Passes	Travel speed ($m.min^{-1}$)	Lead			Trail			Oscillation		CTWD (mm)
		WFS ($m.min^{-1}$)	Current (A)	Volts. (V)	WFS ($m.min^{-1}$)	Current (A)	Volts. (V)	Freq. (Hz)	Osc. width	
Root pass	0.9	11	191.3	20.9	11	178.2	22.1	350	90	14
Fill 1	0.9	12	193.9	20.8	12	170.7	22.7	350	135	14
Fill 2	0.9	13	199.3	21.9	13	182.3	21.7	350	190	14
Fill 3	0.9	14	206.6	22.9	14	195.9	21.3	350	225	14
Fill 4	0.9	15	221.7	22.9	15	184.4	23.1	350	270	14
Cap pass	0.7	13	215.0	21.5	13	178.7	20.9	350	400	14

Table 6. Welding parameters on narrow groove welds of 304L stainless steel plate

Passes	Travel speed ($m.min^{-1}$)	Lead			Trail			Oscillation		CTWD (mm)
		WFS ($m.min^{-1}$)	Current (A)	Volts. (V)	WFS ($m.min^{-1}$)	Current (A)	Volts. (V)	Freq. (Hz)	Osc. width	
Root pass	0.9	11	218.9	21.1	11	21.0	22.1	350	90	14
Fill 1	0.9	12	232.2	21.9	12	230.3	22.3	350	135	14
Cap pass	0.7	10	222.5	23.5	10	219.8	23.9	350	400	14

2.2.2. Local Mechanical Tensioning (Rolling)

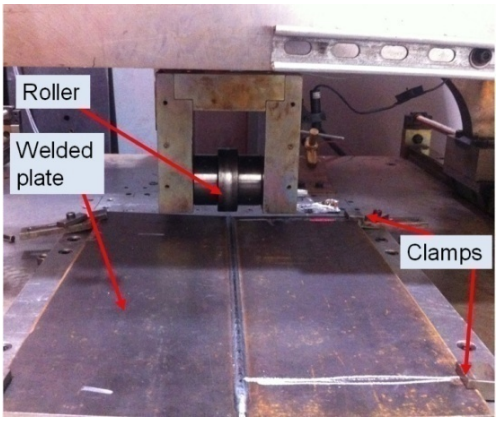

Figure 4. Photograph of the rolling set-up

After welding, local mechanical tensioning by cold rolling was applied to the welded sample. The in-house rolling machine was capable of rolling with a constant force. The principle of operation of this machine is that, the hydraulic cylinder applies a vertical force through a single roller supported in a fork assembly. The roller is made from hardened BS 4659 BH13 tool steel. It has an effective width of 30 mm and its diameter is 100 mm. The welded plate were firmly clamped on the base plate of the rolling rig as shown in Figure 4, while the crossbeam with the roller, is translated by a linear drive system. Post weld cold rolling was carried out on the capping pass of the multi-pass welds using a rolling load of 150 kN for API X100 steel and 100 kN for 304L stainless steel with constant travel speed of 0.7 $m.min^{-1}$. A flat roller was used and under all rolling conditions, the rolling force was applied on the top of the weld metal. The roller did not touch the plate surface on either side of the weld.

2.2.3. Laser Processing

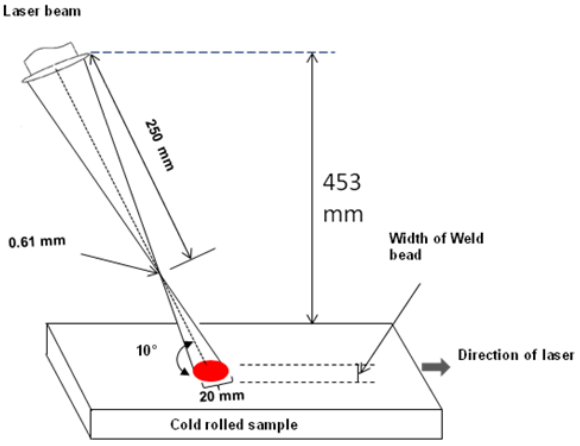

Figure 5. Schematic set-up of laser

As explained before, laser processing was carried out after the rolling process. The laser processing parameters used are designed to ensure that the weld metal was heated to a pre-determined temperature to avoid excessive input of thermal energy. An IPGYLR-8000 fibre laser machine was used and the laser beam was transmitted to the laser head through an optical fibre of 300 µm diameter. Laser beam was collimated using a lens of 125 mm focal length. After

collimating, focussing lens of 250 mm focal length was used to focus the beam. This would produce a spot size of 0.61 mm at the focal point. However, the laser power in this specific experiment was used to increase the temperature at a controlled rate and a defocussed beam of 20 mm spot size was used on the sample surface as shown in Figure 5. The vertical distance for defocussing was determined using a beam diagnostic system. The laser head was positioned at 10^o angle to avoid any back reflection which could damage the lens.

2.3. Experimental Measurement

2.3.1. Weld Thermal Cycles Determination

Thermocouples were used to measure the temperature-time relationship of the weld metal with the aid of a scopecorder 750 instrument. A hole was drilled through the plate thickness (from backing bar) to the weld metal into which K-type thermocouples was placed. The thermocouples were placed at 1.0 mm below the weld cap. Laser power of 3.0 kW with travel speed of 0.3 $m.min^{-1}$ was used for API X100 steel. While laser power of 2.0 kW with laser travel speed of 0.3 $m.min^{-1}$ was used for 304L stainless steel. The difference in laser power was to due to the difference in thermal conductivity of the two materials. Figure 6 shows the sketch of thermocouple positions in weld metal.

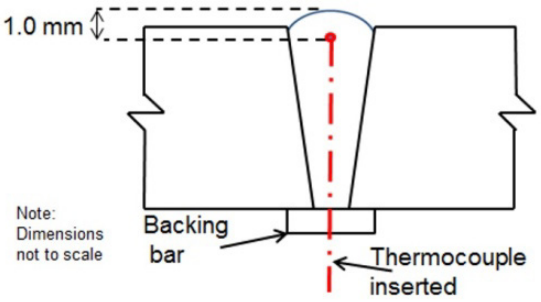

Figure 6. Thermocouple positions in weld metal cross-section

2.3.2. Hardness Test

The welded samples were cut, ground and polished according to standard metallography procedures for microstructural observations and micro hardness tests. For the micro hardness testing, 500 g load and 5 seconds dwell time was applied. Hardness scan was done along the weld metal with an interval of 1.0 mm within successive points.

2.3.3. Measurement of Residual Stresses

SALSA neutron diffractometer at the Institut Laue Langevin in France was used to measure the residual elastic strain [27]. The residual stress state was analysed from the measured elastic strain [28]. Measurements were made on the mid cross-sectional plane of 400 mm sample (plane PQRS) shown in Figure 7. This was based on the assumption that, the stress state in the middle will be from steady state welding condition. The measurements were taken at 2, 10 and 18 mm below the plate surface on which the capping pass was laid for API X100 steel. While for 304L stainless steel, measurements were taken at 2, 6 and 10 mm below the plate surface on which the capping pass was laid. Longitudinal, transverse and normal strains were measured assuming these directions, by symmetry, to be the principal stress directions. The coordinate axes shown as L, T and N in Figure 7, represents the longitudinal (parallel to the length of the weld), transverse (perpendicular to the length of the weld and parallel to the plate) and normal (perpendicular to the length of the weld and perpendicular to the plate) respectively.

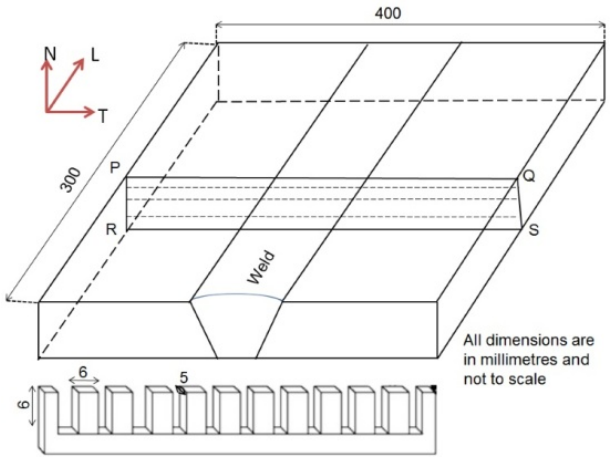

Figure 7. Schematic diagram of the multi-pass welded plate showing lines of measurement with reference comb sample

For API X100 steel, the inter-planar spacing (d) of the {211} crystallographic plane was chosen for measurements of all the principal strain directions. The strain response of {211} family of crystallographic planes in the BCC lattice structure closely follows the macroscopic strain response over the measured gauge volume [27]. While for 304L stainless steel, the inter-planar spacing (d) of the {311} family of crystallographic planes was chosen for measurements of all the principal strain directions since this plane gives the macroscopic average strain over the measured gauge volume [27].

The measurements were made using a neutron incident beam of wavelengths, 1.648 Å, which gives a diffraction angle (2Θ) of 87.62^o and 95.99^o for API X100 and 304L alloys respectively. Through-thickness scan was used for accurate positioning of the gauge volume within the plate. The gauge volume dimension was determined by using slits in front of the in-coming beam and collimating the diffracted beam to maintain the through thickness resolution. An incoming beam of 2 × 2 mm was used for the longitudinal strain measurement while a 2 mm collimator was used for the diffracted beam to achieve the desired spatial resolution. For transverse and normal strain measurement an incoming beam of 2 × 20 mm was used, with the assumption that the stress state and magnitude will remain constant in the welding direction. The increase in gauge volume along the welding direction, in these two

directions, allows faster measurement with more grain sampling.

The stress-free inter-planar spacing was measured using a comb sample of dimension 6 mm × 6 mm × 5 mm machined out from the parent plate by electrical discharge machining (EDM). The dimension of the individual comb would ensure relaxation of any macro residual stress field and will allow positional correction of the measured strain for compositional variation across the weld [29]. The stress-free lattice spacing (d_0) were measured in all the three principal strain directions.

The lattice spacing d is related to scattering angle $\emptyset_{hkl}$ by Bragg's law as shown in equation 1.

$$\{\lambda\} = \left[2d_{hkl}\sin\left(\frac{\phi_{hkl}}{2}\right)\right] \quad (1)$$

Where λ is the wavelength

Gaussian fitting routine was used to fit the intensity profile and precise determination of the peak position. The stress-free lattice spacing (d_0) measurement combined with the lattice spacing measurements were used to calculate strain (ε) using equation 2.

$$\{\varepsilon_{hkl}\} = \left[\frac{(d_{hkl} - d_{0hkl})}{d_{0hkl}}\right] \quad (2)$$

Where ε is strain, d is the lattice spacing of {hkl} family of crystallographic planes, and d_0 is the strain- free spacing (measured in the same plane).

Once the strain is determined, the principal stress could be analysed using the Hooke's law for three dimensional state of stress as shown in equation 3, using the appropriate elastic constants for the specific crystallographic plane.

$$\{\sigma_{ii}\} = \frac{E}{(1+\upsilon)}\left[\varepsilon_{ii} + \frac{\upsilon}{(1-2\upsilon)}(\varepsilon_{11} + \varepsilon_{22} + \varepsilon_{33})\right] \quad (3)$$

Where E and υ are the plane specific Young's modulus and Poisson ratio respectively, and i, = 1, 2, 3 indicate the component of stress and strain relative to chosen to the principal strain directions. Elastic constants values of E = 225.5 GPa and υ = 0.28 [30] for API X100 steel and E = 200 GPa and υ = 0.27 [31], for 304L stainless steel are used to calculate stress from measured strains.

3. Results and Discussions

The transient thermal cycle is described in section 3.1 of this paper. The hardness and residual stresses profile as obtained in the two alloys are described in sections 3.2 and 3.3 respectively.

3.1. Time - Temperature Plot

Figure 8 shows the weld thermal cycle for different laser power and travel speed at constant beam diameter of 20 mm. As shown in the figure, the peak temperature of 3.0 kW at 1.0 mm below the weld surface using a travel speed of 0.3 m.min^{-1} was approximately 759^{o}C (1032 K). With the laser power of 2 kW using the same travel speed and the same position in the weld, the peak temperature was approximately 619^{o}C (892 K). The laser processing parameter was chosen keeping in consideration that excessive heat would reinstate the residual stress state while too low thermal input would be insufficient to induce recrystallisation.

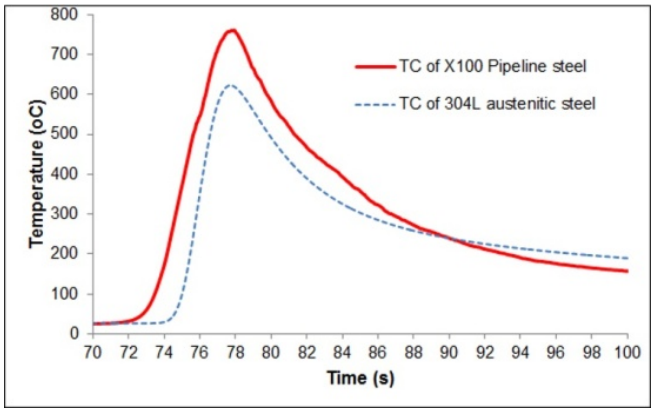

Figure 8. Thermal cycles of laser power 3 kW and 2 kW with travel speed of 0.3 m.min^{-1}

3.2. Hardness

Hardness scan was performed from the reinforcement bead (cap pass) to the root pass of API X100 steel as shown in Figure 9. In the API X100 steel, the effect of cold working was observed up to about 8 mm below the weld cap. Up to about 4 mm the effect is more pronounced after that from 4-8 mm the effect is less pronounced. The as-welded plate shows an increase in hardness value from the cap to the root pass of the weld metal, which suggests thermal straining by successive passes. Hardness scan performed from the cap pass to the root pass of 304L stainless steel is shown in Figure 10. The effect of cold working was observed throughout the entire thickness of the material. Just like the API X100 steel, up to about 4 mm below the cap, the effect is very significant. The effect cold working observed throughout the entire thickness of 304L stainless steel could be attributed to the closely packed crystal structure and large number of active slip systems in the FCC alloy.

Post weld cold rolling followed by laser processing of the API X100 steel resulted in softening of the weld metal up to about 7 mm below weld surface but as hardening, the softening is also more pronounced up to 4 mm (396HV to 300HV). However, post weld cold rolled followed by laser processing of the 304L stainless steel resulted in lesser decrease in the hardness value (300HV to 280HV) of the weld metal. This indicates that the thermal energy applied was not sufficient to supply enough energy for complete recrystallization. The minor scattering in hardness could be due to microstructural variation from re-heating by subsequent passes.

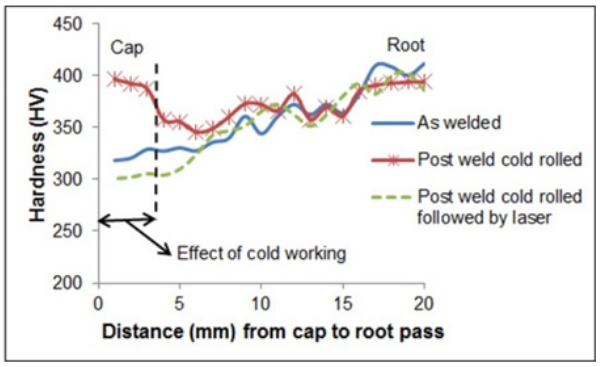

Figure 9. Hardness profile of X100 pipeline steel along the weld metal of the three conditions

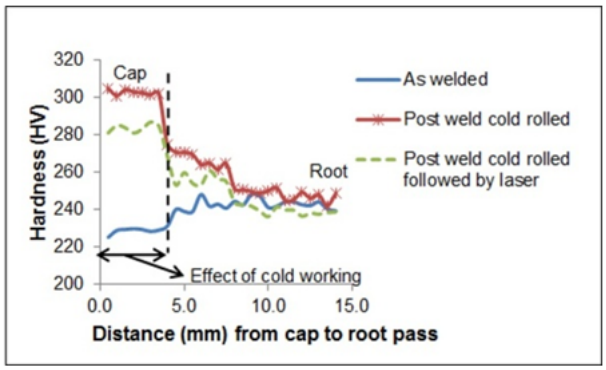

Figure 10. Hardness profile of 304L austenitic steel along the weld metal of the three conditions

3.3. Residual Stress

Due to the nature of heat flow in a welding process, the large magnitude tensile residual stresses are formed parallel to the welding direction and close to the weld zone. As a result, the authors' discussion is focussed on the longitudinal direction. The residual stress analysed from the measurements of elastic strain shows a familiar variation of longitudinal (σ_{xx}) residual stress across the weld. Figure 11 shows the longitudinal stress distribution in API X100 steel at 2 mm below the weld surface. Figure 12 shows the longitudinal stress distribution in 304L stainless steel at identical position.

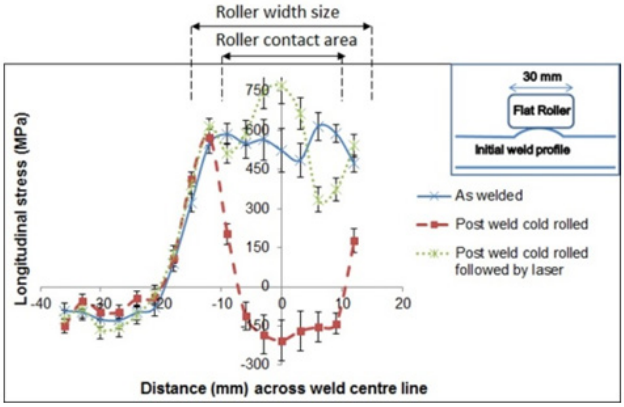

Figure 11. Residual stress profile across the weld in sample with different processing conditions of API X100 steel at 2 mm below the top surface

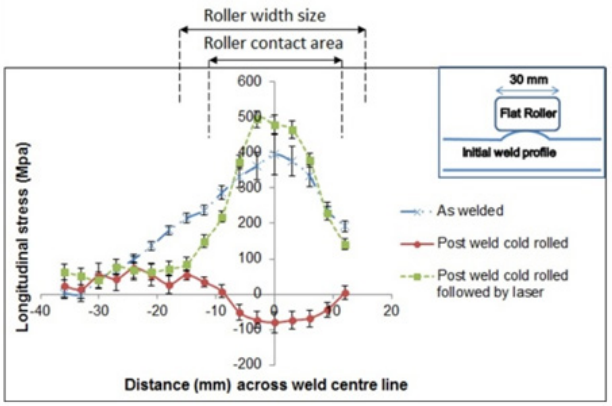

Figure 12. Residual stress profile across the weld in sample with different processing conditions of 304L stainless steel at 2 mm below the top surface

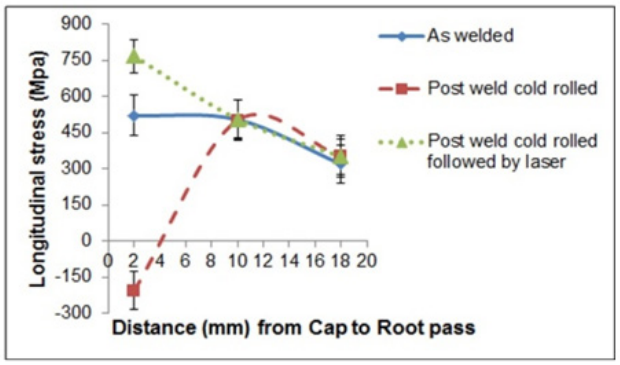

Figure 13. Variation of peak residual stress magnitude through the thickness of API X100 steel (measured at 2, 10, and 18 mm below the top surface)

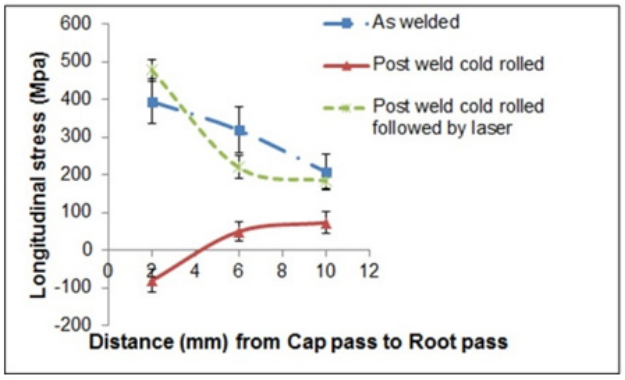

Figure 14. Variation of peak residual stress magnitude through the thickness of 304L stainless steel (measured at 2, 6, and 10 mm below the top surface)

The residual stress analysed from the measurements of elastic strain through the thickness in both alloys showed a reduction in magnitude from cap to root pass in the as-welded state. Post weld cold rolling resulted in localised plastic deformation whereby the tensile residual stress state near the capping pass in the as-welded samples were redistributed as compressive residual stress. As shown in Figure 13 and Figure 14, up to about 4 mm below the weld surface, compressive residual stress was observed. The peak tensile residual stress in the as-welded samples (Figure 13 and Figure 14) diminishes in magnitude through the

thickness. This is attributed to the fact that, multiple passes result in thermal straining of previously laid pass from successive passes. The thermal cycling would cause macroscopic plastic deformation of previously laid passes.

3.3.1. Effect of Post Weld Cold Rolling through the Thickness

A flat roller of 30 mm width was used which determines the extent to which localised plastic strain is induced and thereby, generation of compressive longitudinal stress in both alloys at the cap pass (Figure11 and Figure 12). However, the compressive zone width is narrower than the width of roller because the contact area of the roller is smaller compared to the width of roller. Hence rolling causes plastic deformation around that region of the weld which is approximately 20 mm wide.

Post weld cold rolling of API X100 steel (Figure 11) has changed the longitudinal residual stress state causing it to become compressive around the weld metal (from peak tensile stress of 522 MPa to compressive stress of 205 MPa). Application of rolling to the welded joints causes yielding of material in the weld region, thereby, relieving the residual stresses that exists in the region. Generation of compressive stress state is beneficial in improving the structural integrity of a component as it reduces defect formation. The rolling process, applies a compressive load in the normal direction, thereby causing it to expand in the plane of the weld, relaxing any tensile residual stresses in the plane. Similar effect was observed on 304L stainless steel, changing the peak tensile stress of 395 MPa to compressive stress of 80 MPa (Figure 12).

It was observed that, at about 10 mm below the weld surface of API X100 steel (Figure 13); the rolling load has little influence on the residual stress state of the weld. The rolling changes the peak tensile stress from 505 MPa to 495 MPa suggesting little impact of the rolling in that region. In the case of 304L stainless steel, it was evident that, at about 6 mm below the weld surface (Figure 14), the rolling load has significant influence on the residual stress state of the weld (changing the peak tensile stress from 319 MPa to 50 MPa). These suggest that, the larger number of slip systems available in the FCC structure make it easier to deform the alloy plastically through the thickness which enables reduction of tensile residual stress state.

As evident in Figure 13, at 18 mm below the weld surface of API X100 steel, the rolling load did not show any change in the residual stress state as expected. However, for 304L stainless steel, at 10 mm below the surface (Figure 14) the rolling load changed the peak residual stress to 74 MPa which was 208 MPa in as-welded state. Therefore, the impact of cold rolling progressively reduced through the thickness.

It can therefore be deduced from this work that post weld rolling was effective in significant modification of the residual stress state up to 4 mm below the weld surface in API X100 steel whereas, in 304L stainless steel, the post weld rolling was effective throughout the entire thickness.

3.3.2. Effect Post Weld Cold Rolling Followed by Laser Processing

Laser processing after cold rolling (measurement was taken at 2 mm below the weld surface) for API X100 steel has been shown to increase the longitudinal residual stress from compressive stress of 205 MPa to peak tensile stress of 770 MPa (Figure 11) indicating a high thermal input. Similarly, at 2 mm below the weld surface of 304L stainless steel, an increase in longitudinal residual stress from compressive stress of 80 MPa peak to tensile stress of 479 MPa was observed (Figure 12).

However, at about 10 mm below the weld surface of API X100 steel, laser processing after cold rolling did not show any change in the residual stress state. Indicating that, the heat conducted through the material at that region was not sufficient to cause any changes in the residual stress state. While in the case of 304L stainless steel (6 mm below weld surface), laser processing after cold rolling, a change on longitudinal residual stress state was observed, modifying the peak tensile stress from 50 MPa to 220 MPa (Figure 14). This could be attributed to low thermal conductivity and high coefficient of thermal expansion of the austenitic steel.

In the same way, at about 18 mm below the weld surface of API X100 steel, laser processing after cold rolling did not show any change in the residual stress state. Laser processing to the cold rolled of 304L stainless steel (10 mm below the weld surface) has reinstated residual stress distribution profile to as-welded state.

4. Conclusions

Comparative study of evolution of residual stress state by local mechanical tensioning and laser processing of ferritic (API X100 steel) and austenitic (304L stainless steel) structural steel welds has been investigated. From this experiment, it can be concluded that;

Post weld cold rolling was effective in modifying the residual stress state up to 4 mm below the weld surface of the API X100 steel. Whereas, in 304L stainless steel, the effect of post weld cold rolling was effective in modifying the residual stress state throughout the entire thickness. This difference in these two alloys could be due to the fact that the larger number of slip systems available in the FCC structure (304L stainless steel) make it easier to deform the alloy plastically through the thickness which enables reduction of tensile residual stress state.

As the modification of stress state is achieved by localised plastic deformation, an increase in hardness of the weld metal was observed in both alloys.

The post weld cold rolling followed by laser processing at the cap pass of the two alloys, resulted in reinstated as-welded residual stress state profile. Following this observation, future processing route was identified which is presently under investigation. This new route involves cold

rolling followed by application of high thermal energy which will be sufficient to sustain a complete recrystallization kinetic. This would be followed by another cold rolling to redistribute and eliminate the tensile residual stress state which will form in laser processing.

In both materials, peak tensile residual stress of the as-welded sample diminishes in magnitude through the thickness of a multi-pass weld. This is due to the fact that, multiple passes result in thermal straining of previously laid pass from successive passes. The thermal cycling would cause macroscopic plastic deformation of previously laid passes.

ACKNOWLEDGEMENTS

The authors are grateful for the funding provided by Petroleum Development Trust Fund in Nigeria, under the PTDF scholarship scheme no. PTDF/E/OSS/PHD/SJ/391/11. Dr Supriyo Ganguly acknowledges support from EPSRC through grant numbers EP/J017086/1 and EP/K030884/1.

REFERENCES

[1] Withers, P. J. (2007), "Residual stress and its role in failure", Reports on Progress in Physics, vol. 70, no. 12, pp. 2211-2264.

[2] Dong, P. and Brust, F. W. (2000), "Welding residual stresses and effects on fracture in pressure vessel and piping components: a millennium review and beyond", Journal of Pressure Vessel Technology, Transactions of the ASME, vol. 122, no. 3, pp. 329-338.

[3] Zhang, J. and Dong, P. (2000), "Residual stresses in welded moment frames and implications for structural performance", Journal of structural engineering New York, N.Y., vol. 126, no. 3, pp. 306-315.

[4] Cheng, X., Fisher, J. W., Prask, H. J., Gnäupel-Herold, T., Yen, B. T. and Roy, S. (2003), "Residual stress modification by post-weld treatment and its beneficial effect on fatigue strength of welded structures", International Journal of Fatigue, vol. 25, no. 9-11, pp. 1259-1269.

[5] Fricke, W. (2005), "Effects of residual stresses on the fatigue behaviour of welded steel structures", Materialwissenschaft und Werkstofftechnik, vol. 36, no. 11, pp. 642-649.

[6] Lidbury, D. P. G. (1984), "The significance of residual stresses in relation to the integrity of LWR pressure vessels", International Journal of Pressure Vessels and Piping, vol. 17, no. 4, pp. 197-328.

[7] Read, D. T. (1989), "Measurement of applied J-integral produced by residual stress", Engineering Fracture Mechanics, vol. 32, no. 1, pp. 147-153.

[8] Turski, M., Bouchard, P. J., Steuwer, A. and Withers, P. J. (2008), "Residual stress driven creep cracking in AISI Type 316 stainless steel", Acta Materialia, vol. 56, no. 14, pp. 3598-3612.

[9] Bouchard, P. J., Withers, P. J., McDonald, S. A. and Heenan, R. K. (2004), "Quantification of creep cavitation damage around a crack in a stainless steel pressure vessel", Acta Materialia, vol. 52, no. 1, pp. 23-34.

[10] Turski, M., Francis, J. A., Hurrell, P. R., Bate, S. K., Hiller, S. and Withers, P. J. (2012), "Effects of stop-start features on residual stresses in a multipass austenitic stainless steel weld", International Journal of Pressure Vessels and Piping, vol. 89, pp. 9-18.

[11] Ainsworth, R. A. (2006), "R5 procedures for assessing structural integrity of components under creep and creep-fatigue conditions", International Materials Reviews, vol. 51, no. 2, pp. 107-126.

[12] Lei, Y., O'Dowd, N. P. and Webster, G. A. (2000), "Fracture mechanics analysis of a crack in a residual stress field", International Journal of Fracture, vol. 106, no. 3, pp. 195-216.

[13] Ainsworth, R. A., Sharples, J. K. and Smith, S. D. (2000), "Effects of residual stresses on fracture behaviour - experimental results and assessment methods", Journal of Strain Analysis for Engineering Design, vol. 35, no. 4, pp. 307-316.

[14] Smith, D. J. and Garwood, S. J. (1992), "Influence of postweld heat treatment on the variation of residual stresses in 50 mm thick welded ferritic steel plates", International Journal of Pressure Vessels and Piping, vol. 51, no. 2, pp. 241-256.

[15] Porowski, J. S., O'Donnell, W. J., Badlani, M. L. and Hampton, E. J. (1990), "Use of the mechanical stress improvement process to mitigate stress corrosion cracking in BWR piping systems", Nuclear Engineering and Design, vol. 124, no. 1-2, pp. 91-100.

[16] Richards, D. G., Prangnell, P. B., Williams, S. W. and Withers, P. J. (2008), "Global mechanical tensioning for the management of residual stresses in welds", Materials Science and Engineering A, vol. 489, no. 1-2, pp. 351-362.

[17] Jurcius, A. and Valiulis, A. V. (2008), "Reduce of material residual stresses using vibration energy", Vibroengineering 2008 - Proceedings of 7th International Conference, pp. 50-54.

[18] Rao, D., Chen, L. and Ni, C. (2006), "Vibratory stress relief of welded structure in China", Materials at High Temperatures, vol. 23, no. 3-4, pp. 245-250.

[19] Yanagida, N. and Koide, H. (2006), "Residual stress improvement in multi-layer welded plates using water-shower cooling during welding process", Nihon Kikai Gakkai Ronbunshu, A Hen/Transactions of the Japan Society of Mechanical Engineers, Part A, vol. 72, no. 11, pp. 1631-1638.

[20] Altenkirch, J., Steuwer, A., Withers, P. J., Williams, S. W., Poad, M. and Wen, S. W. (2009), "Residual stress engineering in friction stir welds by roller tensioning", Science and Technology of Welding and Joining, vol. 14, no. 2, pp. 185-192.

[21] Kurkin, S. A. and Anufriev, V. I. (1984), "Preventing distortion of welded thin-walled members of AMg6 1201 Aluminium alloys by rolling the weld with a roller behind the welding arc.", Welding Production (English translation of Svarochnoe Proizvodstvo), vol. 31, no. 10, pp. 52-55.

[22] Kurkin, S. A. and Anufriev V.I. Milekhin, E. S. (1980), "Improving the mechanical properties of welded joints in the AMg6 alloy by plastic deformation during arc welding, svarochnoe proizvodstvo,", vol. 27, pp. 20 - 24.

[23] Liu, W., Tian, X. and Zhang, X. (1996), "Preventing weld hot cracking by synchronous rolling during welding", Welding Journal (Miami, Fla), vol. 75, no. 9, pp. 297-s.

[24] Coules, H. E., Colegrove, P., Cozzolino, L. D., Wen, S. W., Ganguly, S. and Pirling, T. (2012), "Effect of high pressure rolling on weld-induced residual stresses", Science and Technology of Welding and Joining, vol. 17, no. 5, pp. 394-401.

[25] Hudson, M. G. (2004), "Welding of X100 Linepipe (PhD Thesis thesis)", Cranfield University, Cranfield, UK.

[26] Theocharis, L. (2007), "Tandem Gas Metal Arc Pipeline Welding (PhD Thesis thesis)", Cranfield University, Cranfield University.

[27] Pirling, T., Bruno, G. and Withers, P. J. (2006), "SALSA-A new instrument for strain imaging in engineering materials and components", Materials Science and Engineering A, vol. 437, no. 1, pp. 139-144.

[28] Withers, P. J., Turski, M., Edwards, L., Bouchard, P. J. and Buttle, D. J. (2008), "Recent advances in residual stress measurement", International Journal of Pressure Vessels and Piping, vol. 85, no. 3, pp. 118-127.

[29] Haigh, R. D., Hutchings, M. T., James, J. A., Ganguly, S., Mizuno, R., Ogawa, K., Okido, S., Paradowska, A. M. and Fitzpatrick, M. E. (2013), "Neutron diffraction residual stress measurements on girth-welded 304 stainless steel pipes with weld metal deposited up to half and full pipe wall thickness", International Journal of Pressure Vessels and Piping, vol. 101, pp. 1-11.

[30] Coules, H. E., Cozzolino, L. D., Colegrove, P., Ganguly, S., Wen, S. W. and Pirling, T. (2012), "Neutron Diffraction Analysis of Complete Residual Stress Tensors in Conventional and Rolled Gas Metal Arc Welds", Experimental Mechanics, vol. 53, no. 2, pp. 195-204.

[31] William, D. C. (2007), "Material science & engineering; an introduction", 7th ed, USA.